Methanol Synthesis by Hydrogenation of Hybrid CO2−CO Feeds

Originally published in:
ChemSusChem 14(14), https://doi.org/10.1002/cssc.202100859

Methanol Synthesis *via* Hydrogenation of Hybrid CO_2-CO Feeds

Thaylan P. Araújo,[a] Adrian H. Hergesell,[a] Dario Faust-Akl,[a] Simon Büchele,[a] Joseph A. Stewart,[b] Cecilia Mondelli,*[a] and Javier Pérez-Ramírez*[a]

[a] T.P. Araújo, A.H. Hergesell, D. Faust-Akl, S. Büchele, Dr. C. Mondelli, Prof. Dr. J. Pérez-Ramírez
Department of Chemistry and Applied Biosciences
Institute for Chemical and Bioengineering
Vladimir-Prelog-Weg 1, 8093 Zurich (Switzerland)
E-mails: cecilia.mondelli@chem.ethz.ch; jpr@chem.ethz.ch
[b] Dr. J.A. Stewart
Total Research & Technology Feluy
Zone Industrielle Feluy C, 7181 Seneffe, (Belgium)

Supporting information for this article is given via a link at the end of the document.

Abstract: The impact of carbon monoxide on CO_2-to-methanol catalysts has been scarcely investigated, although CO will comprise up to half of the carbon feedstock, depending on CO_2 origin and process configuration. Herein, copper-based systems and ZnO-ZrO_2 were assessed in cycle experiments with hybrid CO_2-CO feeds and their CO sensitivity was compared to In_2O_3-based materials. All catalysts were promoted upon CO addition. Copper-based systems are intrinsically more active in CO hydrogenation and profit from exploiting this carbon source for methanol production, whereas CO induces a surplus formation of oxygen vacancies, *i.e.*, the catalytic sites, on ZnO-ZrO_2, alike In_2O_3-based systems. Mild-to-moderate deactivation occurred upon re-exposure to CO_2-rich streams due to water-induced sintering for all catalysts except ZnO-ZrO_2, which responds reversibly to feed variations likely owing to its more hydrophobic nature and the atomic mixing of its metal components. Our study categorizes catalytic systems for operation in hybrid CO_2-CO feeds, emphasizing the significance of catalyst and process design to foster advances in CO_2 utilization technologies.

Introduction

Addressing global warming while meeting the ever-increasing demand for energy, fuels, and chemicals is an enormous challenge currently faced by humanity.[1] In this scenario, methanol synthesis using captured CO_2 and renewable H_2 or CO_2-rich feeds obtained *via* biomass gasification would permit to curb emissions and produce a versatile building block and promising green fuel.[1a-c,2] In spite of the easy retrofitting of available infrastructure in the chemical industry, the implementation of sustainable CO_2-to-methanol ($CO_2 + 3H_2 \leftrightarrow CH_3OH + H_2O$) technologies at a large scale is contingent on the development of highly performing catalysts.[2a,3] Cu-ZnO-Al_2O_3 systems are a mature technology for syngas-based methanol synthesis ($CO + 2H_2 \leftrightarrow CH_3OH$) and have been examined in CO_2 hydrogenation exhaustively.[1a,3b,4] They show high activity, but their selectivity to methanol and stability are compromised by the competitive reverse water-gas shift reaction (RWGS: $CO_2 + H_2 \leftrightarrow CO + H_2O$) and sintering mediated by the water byproduct, respectively. Replacing alumina by zirconia in this ternary system attained considerable gains on both fronts, since the latter increases the catalyst's CO_2 adsorption capability and hydrophobicity.[1a,3b,4a-c,5] Around the mid-2010s, metal oxides with controlled vacancy chemistry were identified as extremely selective, though intrinsically less active, catalytic phases for CO_2 hydrogenation.[1a,3b,5b] Through precision design of carrier and promoters, indium oxide-based catalysts have nonetheless attained a methanol productivity of up to 1 g_{MeOH} h^{-1} g_{cat}^{-1}.[6] ZnO-ZrO_2 solid solutions also displayed remarkable performance (*ca*. 0.7 g_{MeOH} h^{-1} g_{cat}^{-1}), thanks to augmented active sites created by atomic interaction between ZnO and ZrO_2.[5b,7]

Since CO shall be present in industrially-relevant CO_2 hydrogenation streams as an additional carbon source in the feed or as a recycled byproduct, we recently devised a set of experiments cycling between practically significant CO_2/CO ratios (R) to unravel the impact of hybrid feeds in methanol synthesis over In_2O_3-based systems.[8] Distinct beneficial and detrimental mechanisms were revealed, highlighting that some catalysts are optimal to operate only under pure CO_2 hydrogenation conditions, while others thrive when processing mixtures of CO_2 and CO. Studies on commercial and lab-prepared Cu-ZnO-Al_2O_3 catalysts reporting on the use of hybrid feeds in steady-state or cyclic operation apply R ratios (generally >0.5) irrelevant for methanol production based on CO_2-rich streams.[4f,9] As for Cu-ZnO-ZrO_2 and ZnO-ZrO_2 systems, no work inquires their sensitivity to CO co-feeding. This scenario calls for an investigation of these relevant catalytic solids through a similar approach to In_2O_3-based catalysts to compare their industrial viability on a common basis and pinpoint aspects to be sharpened.

Here, we investigated the impact of hybrid CO_2-CO feeds on the performance of representative commercial and lab-made Cu-ZnO-Al_2O_3 systems, and of Cu-ZnO-ZrO_2 and ZnO-ZrO_2 catalysts, in comparison to In_2O_3 in bulk form or carried on monoclinic zirconia. Promotion and deactivation phenomena were evidenced by employing cycle experiments, in which CO_2 is replaced stepwise by CO and *vice versa*. By applying sensible characterization methods, structural and electronic properties rationalizing positive and negative effects of CO on methanol productivity were identified depending on catalyst composition and structure. Overall, this study offers a direct comparison of all key systems for CO_2-based methanol synthesis under practically significant conditions, hinting to crucial properties to refine for their transposition from lab to plant.

Results and Discussion

3.1. Impact of hybrid CO_2-CO feeds on methanol productivity

The impact of hybrid feeds on CO_2-to-methanol was evaluated over commercial samples of Cu-ZnO-Al_2O_3 from Clariant and Johnson Matthey as well as Cu-ZnO-Al_2O_3 and Cu-ZnO-ZrO_2 self-prepared by co-precipitation using an oxalate-gel route, and a ZnO-ZrO_2 solid solution. The oxalate protocol was selected as a preferred method to attain solids free of performance-hampering sodium and carbon impurities, which are hard to remove in spite of intensive washing and the calcination step applied, respectively. All materials were synthesized according to reported synthesis protocols.[7a,5a,9b] Compositional analyses of the fresh catalysts (Tables S1 and S2) confirmed that the typical molar metals' compositions (Cu:Zn:Al or Zr = 6:3:1) and the nominal loading of ZnO (9 wt.% on ZrO_2) were accurately reached. The XRD patterns, pore volumes, and BET surface areas of all fresh solids (Table 1 and Figure 1) were also in agreement with literature data.[4b,f,5a,9a,b]

To assess their sensitivity to CO co-feeding, the catalysts were tested in a continuous-flow setup equipped with four parallel fixed-bed reactors by means of CO_2-CO full cycles (Figure 2a). Specifically, CO_2 in the feed was gradually replaced by CO, *i.e.*, from $R = CO/CO_x = 0$ to 0.5, and then stepwise restored, *i.e.*, from $R = 0.5$ to 0. Pressure, H_2/CO_x ratio, and *WHSV* were kept at commonly applied values for CO_2-to-methanol (5 MPa, 4, and 48,000 $cm^3_{STP}\ h^{-1}\ g_{cat}^{-1}$, respectively), whereas temperature was set at 513 and 593 K for copper-containing catalysts and ZnO-ZrO_2, respectively, to operate all systems under their optimal conditions. Catalytic performances are reported by means of the methanol *STY*, since CO_2 conversion and methanol selectivity cannot be precisely determined without the demanding use of isotopically labelled compounds. In fact, CO_2 can be formed due to CO reacting with lattice oxygen of active or carrier phases (*vide infra*), particularly at higher *R* values, and with the water formed by CO_2 hydrogenation to methanol. Furthermore, variable amounts of CO are produced by the competitive RWGS reaction, which may be hydrogenated to methanol over some of the systems. This does not comprise a limitation considering the purpose of this work, which is contrasting catalyst behaviors under more realistic conditions, whereby the methanol *STY*, here determined as grams of methanol per hour and per gram of catalyst, is the most suited parameter to evaluate productivity. Moreover, values are normalized for each system to contrast their trends in a more direct manner. The performances of bulk In_2O_3 and In_2O_3 supported on monoclinic zirconia (*m*-ZrO_2) by wet impregnation upon equivalent cycles at 553 K are added to the results to enable a straightforward comparison.[8]

The normalized methanol *STY* shows two opposing tendencies over the catalysts in the full cycles (Figure 3). Considering the forward branches, it increases for all Cu-ZnO-Al_2O_3 systems (+5, +5, and, +7% for CuZnAl-JM, CuZnAl-M700, and CuZnAl-ox, respectively) after $R = 0.1$, while Cu-ZnO-ZrO_2 is boosted by 5% but only after $R = 0.4$. A steadily higher promotion emerged for ZnO-ZrO_2 (+17%). In_2O_3-based catalysts displayed contrasting performances, *i.e.*, methanol productivity augmented over In_2O_3/*m*-ZrO_2 (+8%) whereas a negligible promotional effect was evidenced for bulk In_2O_3 (+1%).[8]

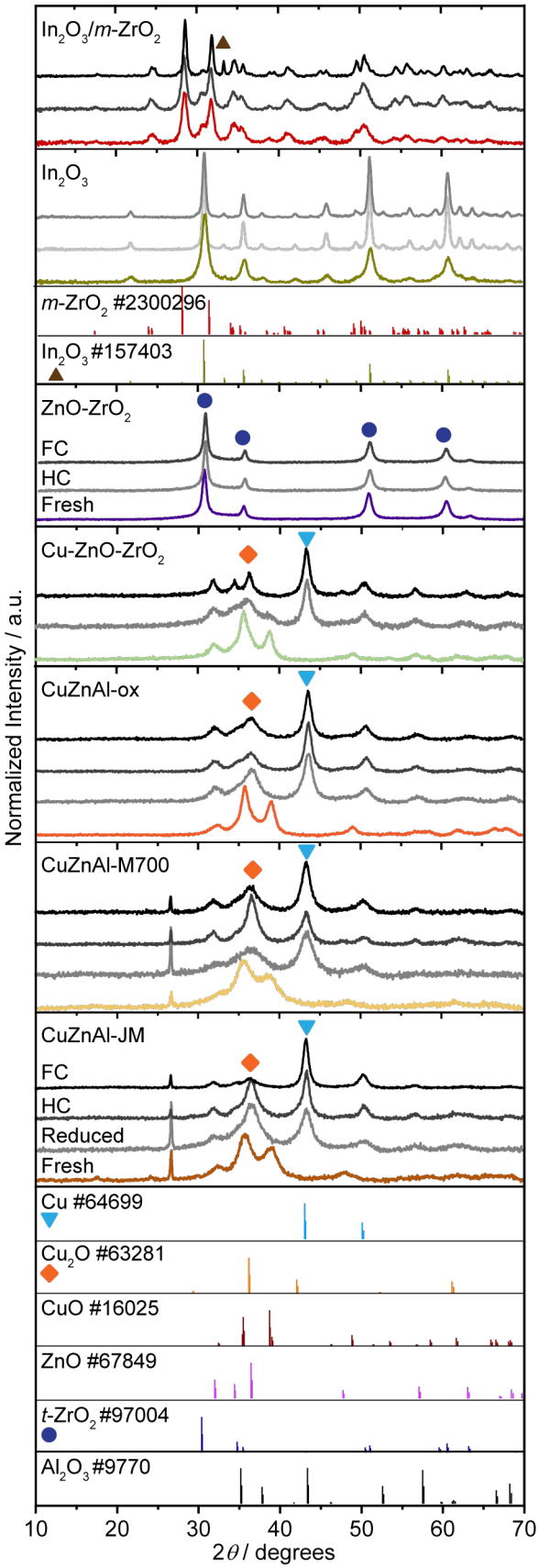

Figure 1. XRD patterns of Cu-ZnO-Al_2O_3, Cu-ZnO-ZrO_2, ZnO-ZrO_2, and In_2O_3-based catalysts in fresh and reduced forms and after use in full cycles (FC) and half-cycles (HC). Reference diffractograms of pure phases are shown with vertical lines.

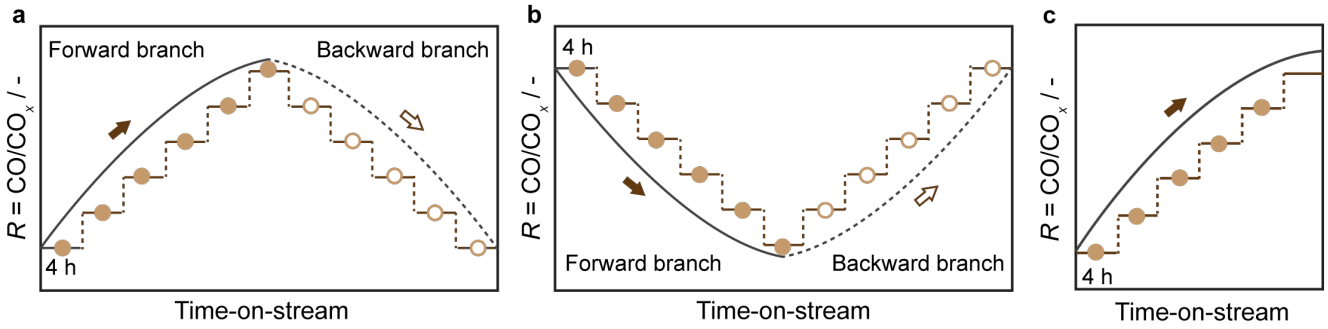

Figure 2. Scheme of the (a) full cycles (FC), (b) reverse full cycles (rFC), and (c) half-cycles (HC) applied in this study to explore the impact of CO on the catalysts in CO_2-based methanol synthesis.

Distinct behaviors were also observed in the backward branches of the cycles (Figure 3). For Cu-ZnO-Al_2O_3 catalysts, the variation in methanol *STY* followed quite closely that in the corresponding forward branches until R = 0.4, 0.2, and 0.1 for CuZnAl-JM, CuZnAl-M700, and CuZnAl-ox, respectively, after which hysteresis is evident. Overall, the methanol productivity decreased similarly for the two commercial catalysts (−12%) and more significantly for CuZnAl-ox (−16%), in all cases respective to the levels previously reached at R = 0.5. Also Cu-ZnO-ZrO_2 showed a hysteresis behavior with a decrease in methanol yield (−21%). This is analogous to In_2O_3 and In_2O_3/*m*-ZrO_2, which experienced strong and mild hysteresis followed by a drop of −25 and −17% in performance, respectively. Differently to these systems, the backward branch for ZnO-ZrO_2 mirrored its forward counterpart, with a drop in methanol *STY* upon returning to R = 0, practically equalling the gain in the forward branch (−15%).

In general, the overall Δ*STY*(A→C, radar plot in Figure 3) in the whole cycle revealed mild-to-moderate levels of deactivation (−5 to −19%) across the catalyst families, except for ZnO-ZrO_2, which remained at a comparable value (+2%). The robustness of the ZnO-ZrO_2 system in hybrid feeds is an advantage for perspective CO_2-to-methanol industrial processes, where the feed composition might fluctuate considerably (R = 0.05 to 0.5) as a result of the CO_2 source adopted (*i.e.*, carbon capture or biomass gasification) and the purging conditions applied to recycled streams.[10] Indeed, ZnO-ZrO_2 could exploit the whole CO_2/CO ratio spectrum without detrimental effects. CuZnAl-M700 and CuZnAl-ox would be suitable for operation at $R \geq 0.2$, whereas CuZnAl-JM and Cu-ZnO-ZrO_2 would be restricted to processes with $R \geq 0.3$ and 0.4, respectively. It is worth noting that, in spite of mild deactivation in the full cycle, In_2O_3/*m*-ZrO_2 displayed stable performance in a 120-h cycle between R = 0 and 0.2 and also after activation in CO/H_2 mixtures followed by testing at R = 0, 0.2 and 0.5, indicating the need for long-term assessment for all best candidates in future research.[8]

Copper-based catalysts are typically more active than observed in our full cycle when processing CO-rich feeds,[4f,9a,b] with the methanol productivity considerably surpassing the sum of the individual rates of pure CO and CO_2 hydrogenation for R = 0.3-0.6.[11] This discrepancy might be explained by the induction period that these systems tend to experience when the feed composition is altered.[4f,12] In this context, CuZnAl-JM and CuZnAl-M700 were additionally tested in reverse full cycles (rFC), *i.e.*, from R = 0.5 to 0 and back to 0.5 (Figures 2b and 4), to better probe their catalytic performance prior to exposure to a CO_2-rich environment. For both systems, the methanol productivity at R = 0.5 was *ca*. 50-80% higher than under the same condition in the full cycles (Figure 3) and decreased as CO was replaced by CO_2 in the feed, in line with the expectations. The value reached at R = 0 is *ca*. 5-10% higher with respect to the same point in the full cycles. Although the methanol productivity raised again when CO was reintroduced to the feed, a similar hysteresis behavior to the full cycles developed for CuZnAl-JM and CuZnAl-M700, implying a performance loss of *ca.* 50% at the end of the reverse cycle. These findings indicate that a start at CO-rich feeds with additional CO being fed prior to adjustment to the process conditions might help to operate copper catalysts more efficiently.

Although after decades of investigations a full consensus has not been reached, the most compelling mechanism for methanol synthesis from syngas over copper-based catalysts includes the conversion of CO into CO_2 through the water-gas shift reaction ($CO + H_2O \leftrightarrow CO_2 + H_2$), which is then transformed into methanol ($CO_2 + H_2 \leftrightarrow CH_3OH + H_2O$).[1] CO addition will thus favor methanol production as it will suppress the reverse water-gas shift reaction ($CO_2 + H_2 \leftrightarrow CO + H_2O$). As for ZnO-$ZrO_2$, studies describing the interconnection of CO and CO_2 hydrogenation and the (reverse) water-gas shift are lacking, with our results point to a limited utilization of added CO for methanol synthesis either *via* direct hydrogenation or though hydrogenation of CO_2 attained *via* the water gas shift reaction. Hence, although methanol productivity is expected to drop or be sustained depending on the carbon feedstock composition, the magnitude of variations in methanol *STY* in the cycles also advocates for alterations in the catalyst structure. Distinct changes of reversible and irreversible nature are anticipated to dictate beneficial and detrimental CO effects on the different catalysts. Accordingly, sintering of copper and/or its accompanying oxides into larger particles shall be responsible for negatively impacting the performance of copper-containing catalysts. Since CO is easily activated and a surplus of oxygen vacancies without loss of surface area is generated on In_2O_3/*m*-ZrO_2 at increasing R values leading to improved performance, the productivity boost over ZnO-ZrO_2, which shares a similar type of active site, is predicted to depend on an equivalent mechanism. For In_2O_3, sintering rationalizes its deactivation.[8] Property-function relations are sought after though in-depth characterization, as detailed hereon.

3.2. Structural origin of promotion and deactivation by CO

To probe changes in structural and electronic features and unravel their contributions to the observed performance alterations, fresh, reduced , and used catalyst samples were

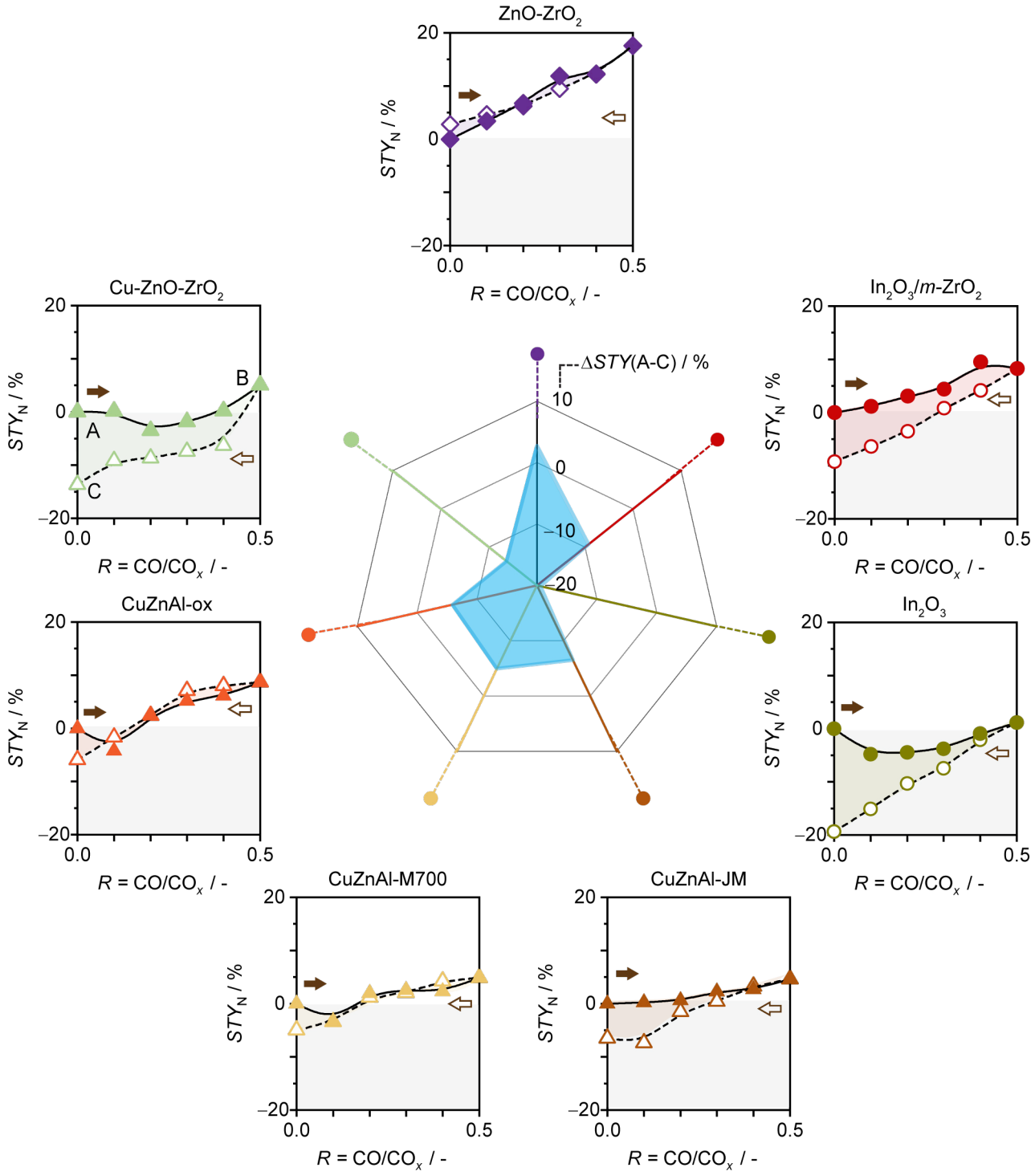

Figure 3. Normalized methanol *STY* during CO_x hydrogenation over Cu-ZnO-Al_2O_3, Cu-ZnO-ZrO_2, ZnO-ZrO_2, and In_2O_3-based catalysts as a function of *R* (*R* = CO/CO_x) in full cycles, where CO_2 in the CO_2+H_2 feed (A) is replaced by CO stepwise (solid symbols) until *R* = 0.5 (B) and then gradually reintroduced (open symbols) back to *R* = 0 (C), and difference of methanol *STY* for the same catalysts at the beginning and the end of the full cycles (radar plot). Data is normalized to the methanol *STY* value displayed by the catalysts at the start of the full cycles. Filled and empty arrows in indicate the forward and backward direction in the full cycles, respectively. Reaction conditions: 513 K for copper-containing, 593 K for ZnO-ZrO_2, and 553 K for In_2O_3-based catalysts, 5 MPa, H_2/CO_x = 4, and 48,000 $cm^3\ h^{-1}\ g_{cat}^{-1}$.

assessed by various techniques. To this end, all catalysts were additionally tested in half-cycles to retrieve samples for characterization (Figure 2c). The surface area (S_{BET}) and pore volume, measured by N_2 sorption (Tables 1 and S1), decreased upon reduction by H_2 for all Cu-ZnO-Al_2O_3 catalysts, as expected, further dropping to distinct levels after their use in the cycles. Specifically, the S_{BET} lowered by about 30% (from 69 and 80 to 52 and 49 $m^2\ g^{-1}$, respectively) for reduced commercial CuZnAl-JM

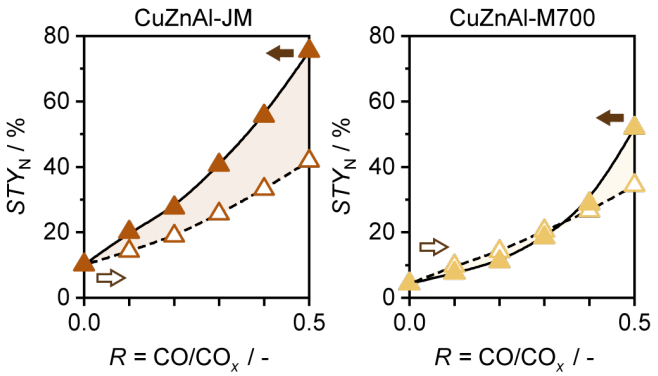

Figure 4. Normalized methanol *STY* during CO_x hydrogenation over Cu-ZnO-Al_2O_3 catalysts as a function of *R* (*R* = CO/CO_x) in reverse full cycles. Data is normalized to the methanol *STY* value displayed by the catalysts at the start of their corresponding full cycles (Figure 3). Filled and empty arrows indicate the forward and backward direction in the reverse full cycles, respectively. Reaction conditions: 513 K, 5 MPa, H_2/CO_x = 4, and 48,000 $cm^3\,h^{-1}\,g_{cat}^{-1}$.

Table 1. Characterization data of the catalysts investigated.

Catalyst	Status[a]	S_{BET}[b] ($m^2\,g^{-1}$)	V_{pore}[c] ($cm^3\,g^{-1}$)	$d_{Cu,XRD}$[d] (nm)
CuZnAl-JM	Fresh	95.9	0.19	–
	Reduced	69.4	0.15	5.2
	HC	51.9	0.15	12.6
	FC	44.0	0.15	13.2
	rFC	65.0	0.15	10.2
CuZnAl-M700	Fresh	81.4	0.23	–
	Reduced	79.8	0.22	4.7
	HC	49.3	0.16	7.0
	FC	51.7	0.22	7.5
	rFC	53.0	0.22	5.6
CuZnAl-ox	Fresh	69.3	0.24	–
	Reduced	67.0	0.17	7.3
	HC	41.4	0.12	10.0
	FC	40.9	0.12	12.4
Cu-ZnO-ZrO_2	Fresh	78.2	0.14	–
	Reduced	58.4	0.12	8.5
	FC	40.8	0.11	8.9
ZnO-ZrO_2	Fresh	42.0	0.05	16.5[e]
	HC	39.7	0.05	18.9[e]
	FC	41.0	0.05	18.1[e]
In_2O_3	Fresh	129	0.41	7.9
	HC	34	0.24	17.3
	FC	28	0.22	18.9
In_2O_3/*m*-ZrO_2	Fresh	81	0.21	–
	HC	82	0.21	–
	FC	76	0.20	–

[a] Data relative to catalysts in fresh and reduced forms and after use in full cycles (FC) and half-cycles(HC). [b] BET method. [c] Single-point pore volume. [d] Determined from the (200) and (111) reflections of metallic copper in the XRD patterns using the Scherrer equation. [e] ZrO_2 crystallite size.

and CuZnAl-M700 and by about 40% (from 69 to 41 $m^2\,g^{-1}$) for CuZnAl-ox after the forward branches of the full cycle, and remained then almost constant after the subsequent backward branch. The sintering behavior of these catalysts is further confirmed by the copper particle size determined by XRD ($d_{XRD,Cu}$, Table 1), which increases from 5.2, 4.7, and 7.3 nm to 13.2, 7.5, and 12.4 nm for CuZnAl-JM, CuZnAl-M700, and CuZnAl-ox, respectively. Notably, copper particles in CuZnAl-JM and CuZnAl-M700 sintered less after the reverse full cycle (to 10.2 and 5.6 nm, respectively), which is in line with their superior performance when starting at CO-richer feeds. In spite of the diminished S_{BET} (from 58 to 41 $m^2\,g^{-1}$), the copper particle size remained unchanged (from 8.5 to 8.9 nm) for Cu-ZnO-ZrO_2, hinting to interparticle porosity becoming lower and/or inaccessible. No significant sintering was observed for the ZnO-ZrO_2 system according to S_{BET} (from 42 to 40 $m^2\,g^{-1}$), pore volume (from 0.048 to 0.046 $cm^3\,g^{-1}$), and ZrO_2 particle size (from 17 to 19 nm). This indicates that the promotion of this system upon CO co-feeding shall be linked to modifications of its surface properties. The behavior of ZnO-ZrO_2 resembles that of In_2O_3/*m*-ZrO_2, which was boosted upon going from *R* = 0 to 0.5 (Figure 3).[8] Both In_2O_3-based catalysts, however, deactivated to some extent due to indium oxide sintering. Indeed, its surface area and pore volume decreased by 79 and 50%, respectively, and the In_2O_3 particle size increased from 8 to 19 nm by the end of the full cycle for the bulk catalyst.[8] Restructuring of the supported material is evidenced by XRD, as detailed below.

XRD patterns of all copper-containing catalysts revealed characteristic reflections around 38 and 42° 2θ due to Cu_2O and metallic Cu, respectively, after treatment in H_2, which remained unchanged after the half-cycles, full cycles, and reverse full cycles (Figures 1 and S1). This corroborates the formation of a Cu-ZnO interface, which is regarded as the active site for methanol synthesis.[4a,c,9b,13] As expected, no changes are evidenced in the diffractograms of ZnO-ZrO_2 upon reduction and after the full cycle with respect to its fresh counterpart (Figure 1). The patterns of In_2O_3 and In_2O_3/*m*-ZrO_2 evidence sintering based on the sharpening of the indium oxide reflections for the former and the appearance of a weak but distinct signal for indium oxide for the latter (Figure 1).

To examine the morphology and relative distribution of the distinct phases in the catalysts, samples were analyzed by HAADF-STEM and chemical element maps were attained by EDX. For Cu-ZnO-Al_2O_3 catalysts, copper and zinc are well distributed within all reduced solids (Figures 5a–c). This is in line with the copper surface area (S_{Cu}) and a copper dispersion (*D*) results (Table S1), which show a rather similar value for these parameters among the systems (S_{Cu} = 22–26 $m^2\,g_{cat}^{-1}$ and *D* = 7–10%). The catalyst architecture remained almost unaltered for CuZnAl-M700 and CuZnAl-ox after the half-cycle, while the copper particle size increased due to moderate sintering for CuZnAl-JM (Figures 5a–c). Interestingly, no copper and ZnO segregation was observed for these systems, which could explain their moderate deactivation, since the active Cu-ZnO interface is not disrupted but only the individual components sintered. Regarding Cu-ZnO-ZrO_2, it possesses a low copper surface area and dispersion (S_{Cu} = 11 $m^2\,g_{cat}^{-1}$ and *D* = 4%) and zinc oxide is not well dispersed on the copper and slightly sinters after the full-cycle, which explains its performance (Figure 5d). As for the ZnO-ZrO_2 solid solution, its structure remains practically unaltered, with no segregated zinc and zirconium oxide phases visible after the cycle experiment, highlighting its robustness (Figure 5e). Indium oxide in In_2O_3/*m*-ZrO_2 retained a rather high dispersion over *m*-ZrO_2 after half-cycles in spite of the moderate sintering also detected by XRD (Figures 1 and 5f).[8]

To assess the reducibility of the catalysts by CO, which is a stronger reducing agent than H_2, CO-TPR measurements were conducted on the fresh samples (Figure 6a). The profiles obtained for Cu-ZnO-Al_2O_3 catalysts reveal a common flat feature starting around 423 K and not falling back to the baseline in the temperature range probed, with maxima at *ca.* 585, 552, and 531 K for CuZnAl-JM, CuZnAl-M700, and CuZnAl-ox, respectively. This signal is due to the superimposed reduction of surface and bulk copper species, as ZnO is generally irreducible

under the conditions applied in the analysis.[9] These characteristic profiles are generally associated with copper sites in close vicinity to ZnO, *i.e.*, the active site for methanol synthesis.[5a,9b] The curve of Cu-ZnO-ZrO_2 is analogous to those of Cu-ZnO-Al_2O_3 samples, reaching a maximum at 540 K. For ZnO-ZrO_2, the CO_2 evolution profile shows three peaks with maxima at 394, 513, and 696 K, indicating ready CO activation at it surface at temperatures even lower than applied in the reaction (593 K), which agrees with literature data. This hints at oxygen vacancy density being augmented upon introducing CO in the feed as well as to the generated CO_2 strongly binding to these sites,[7a] explaining the improved performance upon moving from

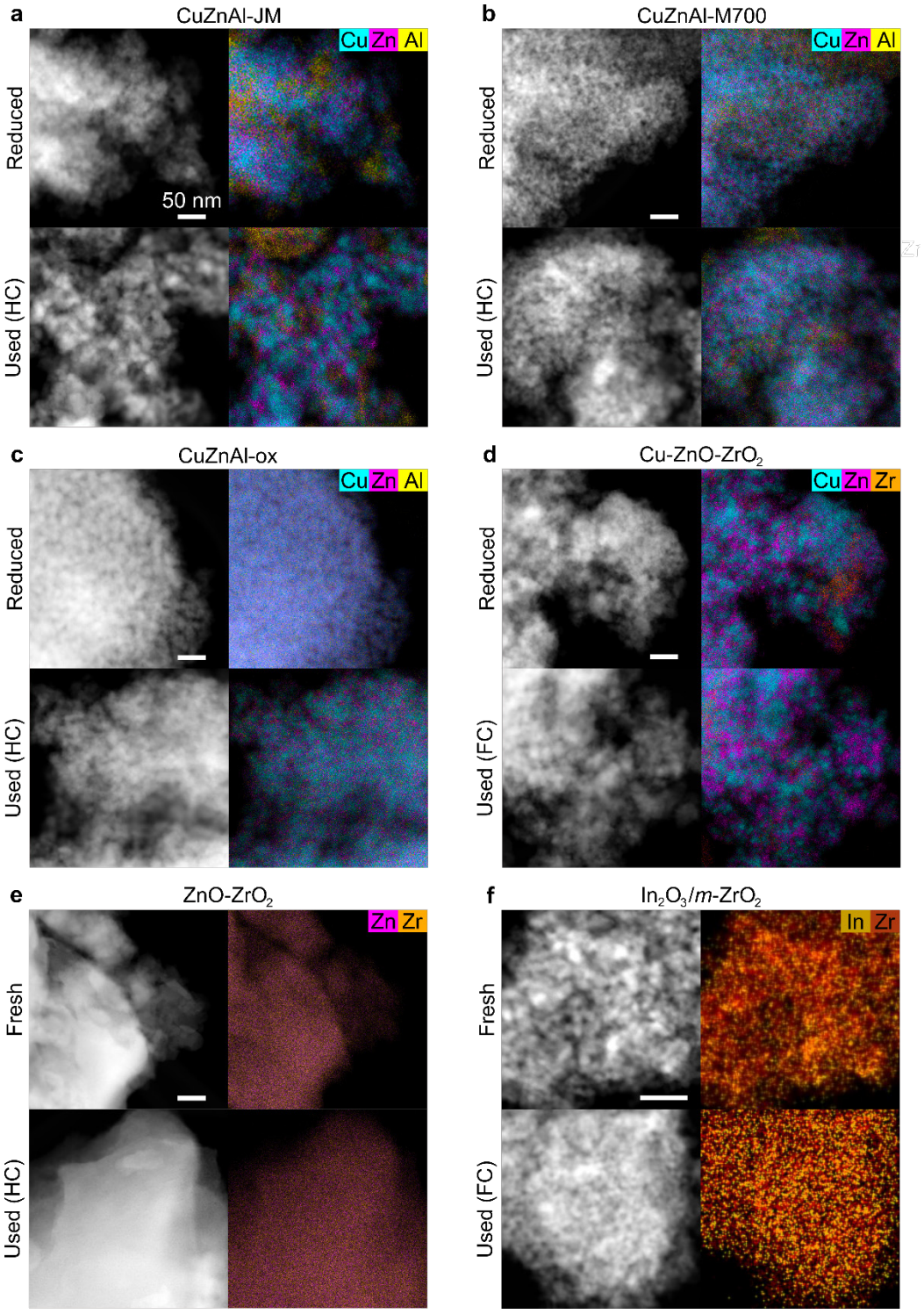

Figure 5. HAADF-STEM micrographs and EDX maps of Cu, Zn, Al, Zr, and In for (a) CuZnAl-JM, (b) CuZnAl-M700, (c) CuZnAl-ox, (d) Cu-ZnO-ZrO_2, (e) ZnO-ZrO_2, and (f) In_2O_3/*m*-ZrO_2 before and after use in full cycles (FC) and half-cycles (HC). The indicated length of the scale bar (50 nm) applies to all micrographs.

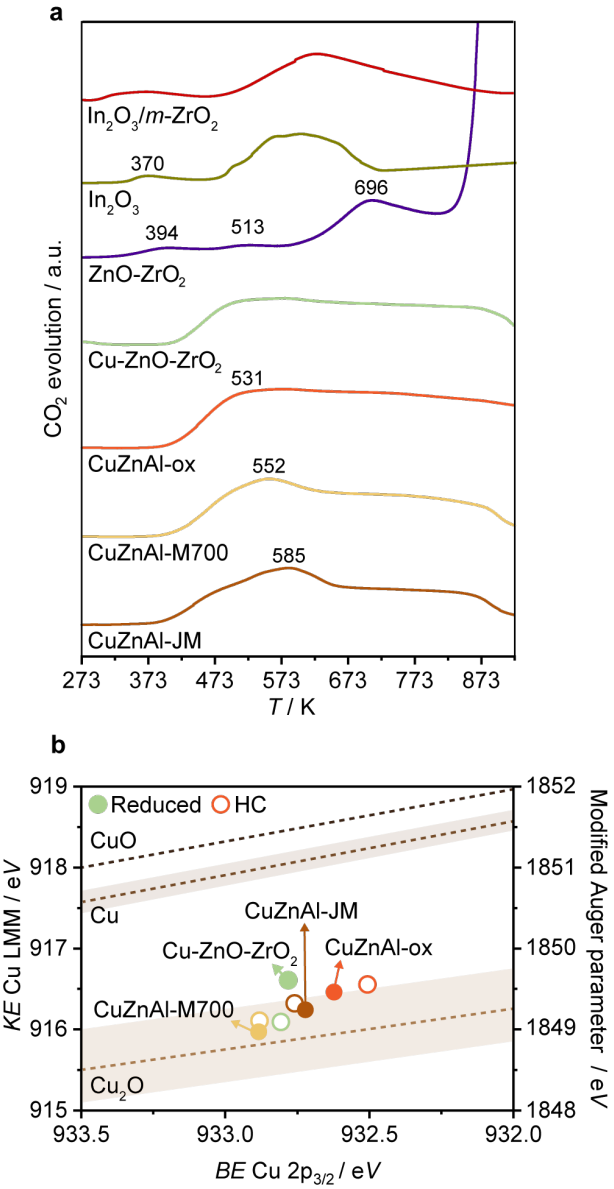

Figure 6. (a) CO-TPR profiles for Cu-ZnO-Al_2O_3, Cu-ZnO-ZrO_2, ZnO-ZrO_2, and In_2O_3-based catalysts and (b) Wagner plot for the copper-containing systems in reduced and used forms. Kinetic and binding energies for copper species were attained from the Cu $2p_{3/2}$ core-level XPS and Cu LMM Auger spectra shown in Figures S2a,b.

R = 0 to 0.5 (Figure 3). The boosted methanol productivity over In_2O_3/m-ZrO_2 was similarly attributed to an increase in the number of vacancies created upon surface reduction of highly dispersed In_2O_3 at *ca.* 553 K, likely aided by the carrier due to the tensile force exerted onto the active phase.[6g,8] The curve of In_2O_3 features two peaks with maxima at *ca.* 370 and 573 K, ascribed to surface and bulk reduction of In_2O_3, respectively.[8]

To gain insights into surface compositions and electronic properties of the metals, the different systems were analyzed by XPS. Although reduced and used copper-based catalysts had to be exposed to air for introduction into the spectrometer, previous literature indicates no major copper oxidation upon this procedure.[4f,9b] In line with this, Cu LMM Auger emission lines (Figure S2b) evidence the presence of metallic Cu and Cu^+ species and the absence of Cu^{2+} cations for all Cu-ZnO-Al_2O_3 systems and Cu-ZnO-ZrO_2.[4a,f,5a] This is supported by the Wagner plot (Figure 6b) derived from the Cu $2p_{3/2}$ core-level emissions and their corresponding Auger lines (Figures S2a,b), and agrees well with the XRD results (Figure 1), showing Cu_2O and Cu as the only copper phases formed upon reduction and reaction. Regarding zinc, Zn LMM Auger emission lines (Figure S2c) revealed no reduction of Zn^{2+} species to any lower state species, which is expected since this metal is known to remain in the form of ZnO.[4b,9b,14] Generally, the surface of all reduced catalysts is richer in copper (*ca.* 53–60 at.%), and becomes richer in zinc upon reaction. Indeed, since copper in CuZnAl-JM and CuZnAl-M700 catalysts sinters (Table 1), while the particle size of zinc oxide remains unaltered, XPS comparatively detects more zinc oxide on the surface of the used materials. CuZnAl-ox comprises an exception, as its reduced sample already possesses a Zn-richer surface (Cu/Zn ratio <1, Table S3), which persists after testing (Table S3). This could explain the lack of hysteresis for this catalyst in the full cycle (Figure 3). For ZnO-ZrO_2, zinc species remained oxidized after the half-cycles and full cycles, as evident by the Zn LMM Auger emission lines (Figure S2c). Also, no significant increase in the surface zinc content was observed for this catalyst after the same tests (Table S4). Similarly, no substantial change in the surface composition of In_2O_3/m-ZrO_2 and In_2O_3 was detected after the half-cycles, which exclusively contained indium in oxidized form (Table S4 and Figure S3).[6l,8,13,15] Since oxygen vacancies are a common active site shared by ZnO-ZrO_2 and In_2O_3-based catalysts, the amount of oxygen atoms next to a defect (O_{defect}) relative to other distinct oxygen species (Table S4) was determined by analyzing the O 1*s* core-level spectra. A considerable alteration in the content of O_{defect} was observed for ZnO-ZrO_2 and In_2O_3/m-ZrO_2 (from 14 to 21 and 22% after the half-cycles, respectively) whereas no significant change occurred on In_2O_3 after the same experiment (from 23 to 22%).[8] These findings are in line with a pronounced and negligible positive role of CO on the performance of the two mixed-oxide catalysts and indium oxide, respectively, upon going from R = 0 to 0.5, which is critically counterbalanced by negative structural changes for the latter.

To provide a comprehensive rationalization of the promotion and deactivation mechanisms acting on most relevant catalysts in CO_2-to-methanol when using hybrid feeds, the key findings attained by performance assessment and characterization are graphically summarized in Figure 7. The beneficial impact of CO on methanol productivity over Cu-ZnO-Al_2O_3 and Cu-ZnO-ZrO_2 catalysts is linked to their intrinsic ability to activate CO to produce methanol and the stability of the Cu-ZnO interface in CO-richer feeds. Sintering of Cu and ZnO phases induced by water triggers their deactivation when CO_2 is restored in the stream and this byproduct is formed in higher amounts. Nonetheless, deactivation could be lessened by first exposing catalysts to less CO_2-rich environments. CO co-feeding augments the density of oxygen vacancies on ZnO-ZrO_2, analogously to In_2O_3-based catalysts. ZnO-ZrO_2 responds fully reversibly to feed composition fluctuations as its structure remains unaltered. The inferior activity of ZnO-ZrO_2 compared to copper-based systems is beneficial in limiting the amount of water byproduct formed that could trigger sintering phenomena. Nonetheless, indium oxide and In_2O_3/m-ZrO_2 display moderate deactivation being similarly active to ZnO-ZrO_2, indicating that intrinsic properties of the latter play an important role in its stable performance. The more pronounced hydrophobic nature and the atomic intermixing of the metals, *i.e.*, the lack of interfaces between components, seem relevant to this

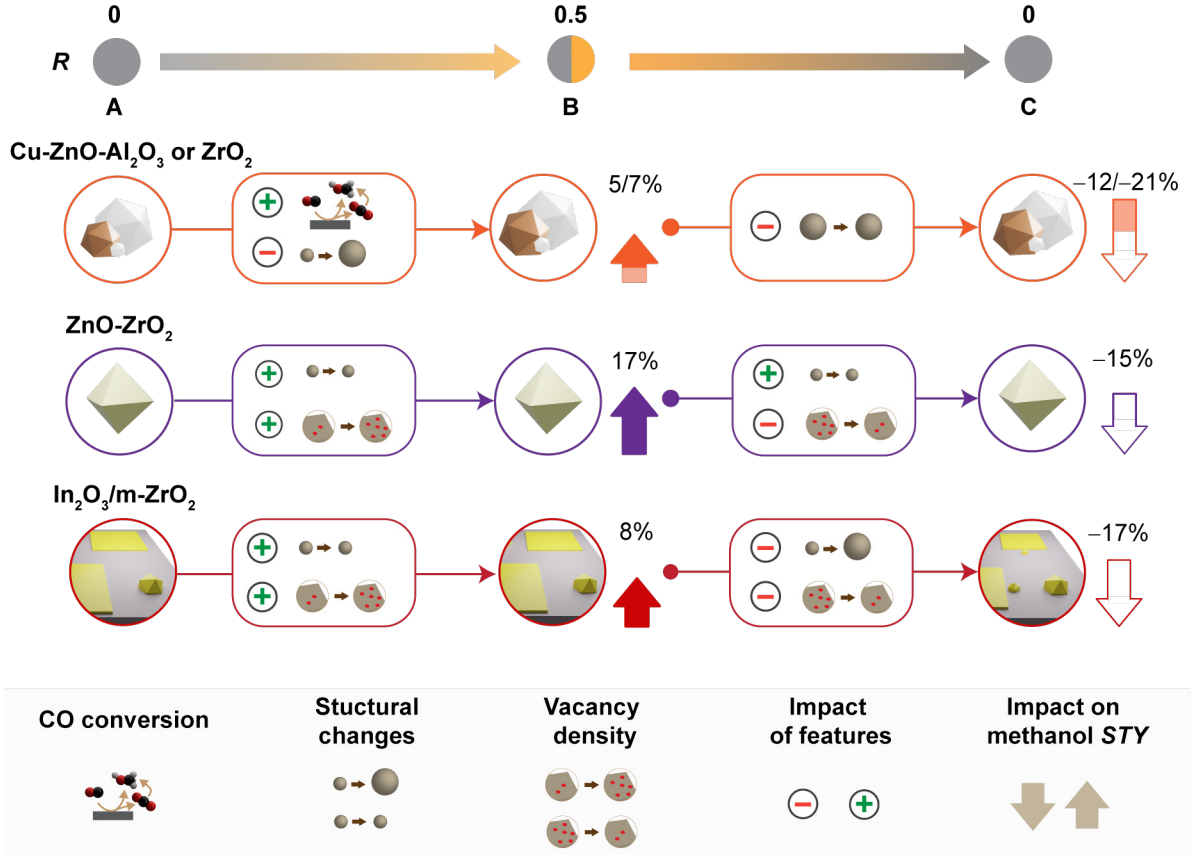

Figure 7. Schematic representation of promotion and deactivation mechanisms along the full cycles for copper-based catalysts, ZnO-ZrO_2, and supported In_2O_3. Models illustrate key structural properties of the catalysts at points A, B, and C of the full cycles (see Figure 3).

end.[16] The first aspect is intrinsic to zirconia and is translated to the solid solution, as water desorption from ZnO-ZrO_2 appears more favorable than from bulk In_2O_3 (0.60 *vs.* 0.88 eV), when two independent studies are compared.[6b,7a] It should also be remarked that the ZnO-ZrO_2 catalyst is operated at a higher temperature (593 *vs.* 553 K for In_2O_3/*m*-ZrO_2), which favors water desorption. Copper- and In_2O_3-based systems will benefit from further catalyst design towards improved stability against feed fluctuations. Moreover, intensified process layouts, featuring reactor configurations integrating removal of water from the reaction mixture, are put forward as an additional sensible strategy to foster a more robust deployment of these catalyst families.

Conclusion

Aiming towards the establishment of CO_2-based technologies for methanol synthesis, this study gathered fundamental knowledge on the sensitivity to CO of Cu-ZnO-Al_2O_3, Cu-ZnO-ZrO_2, and ZnO-ZrO_2 in comparison to In_2O_3 in bulk form and carried on monoclinic zirconia. Upon replacing CO_2 by increasing amounts of CO, in ranges spanning across the composition of practical gaseous feeds, all systems experienced a mild-to-moderate performance improvement. Facile CO hydrogenation on copper-based catalysts and generation of additional oxygen vacancies on ZnO-ZrO_2, analogously to In_2O_3-based systems, were uncovered as the main reasons underpinning promotional phenomena. Upon returning to pure CO_2 hydrogenation conditions, ZnO-ZrO_2 stood out as deactivation particularly robust catalyst. Its characteristic hydrophobicity and the atomic intermixing of the metals were indicated as essential properties to this end, rendering it resistant to water-induced sintering, the major cause for the moderate deactivation of all other catalysts.

Overall, our findings offer a revisited categorization of the most relevant catalyst families for CO_2-to-methanol, uncovering the unique robustness of ZnO-ZrO_2 against feed composition fluctuations in an application-oriented perspective. Future investigations aimed at bridging the gap between lab-based and industrially-viable catalytic technologies for CO_2-to-methanol shall encompass evaluating catalyst stability in practically-relevant feeds in longer-term or accelerated-ageing tests. In addition, catalyst and process design should take center stage to alleviate the detrimental impact of water on the lower-temperature systems, which will ultimately support the development of the many processes in which CO_2 is reduced with hydrogen leading to the generation of this byproduct. A deeper understanding of the interplay of reactions in the network determining the water byproduct using isotopically labelled carbon oxides will also be helpful to this end.

Experimental Section

Catalyst preparation

Commercial pelletized Cu-ZnO-Al_2O_3 methanol synthesis catalysts possessing a typical molar Cu:Zn:Al composition of 6:3:1 were supplied by Alfa Aesar–Johnson Matthey ('copper based methanol synthesis catalyst', LOT I06Z036, denoted as CuZnAl-JM) and Clariant (MegaMax700, LOT 102090, denoted as CuZnAl-M700). Ternary Cu-ZnO-Al_2O_3 and Cu-ZnO-ZrO_2 catalysts (denoted as CuZnAl-ox and CuZnZr-ox, respectively) featuring the same relative metals' content as the commercial materials were prepared *via* oxalate-gel coprecipitation according to reported methods.[5a,9b] Briefly, 114 cm^3 of a 1 M solution containing the required metal nitrates ($Cu(NO_3)_2{\cdot}3H_2O$ (Sigma-Aldrich, 98%), $Zn(NO_3)_2{\cdot}6H_2O$ (Acros Organics, 98%), and $Al(NO_3)_2{\cdot}9H_2O$ (Sigma-Aldrich, 98%) or $ZrO(NO_3)_2{\cdot}6H_2O$ (Sigma-Aldrich, 99%)) in ethanol (99.8%, Fisher Scientific) was quickly mixed with 136 cm^3 of a 2 M solution of oxalic acid (98%, Acros Organics) in ethanol (2 M) under magnetic stirring (*ca.* 500 rpm) at 303 K. After further stirring for 5 min, the obtained gel was isolated by vacuum filtration, washed 3 times with ethanol (1 L each time), dried in a vacuum oven (2 kPa, 323 K, 12 h), and calcined at 573 K (heating rate = 2 K min^{-1}) for 4 h in static air.

A ZnO-ZrO_2 solid solution with a molar Zn:Zr composition of 13:87 was prepared following a reported procedure.[7a] Briefly, 200 cm^3 of a 0.16 M aqueous solution of $Zn(NO_3)_2{\cdot}6H_2O$ and $ZrO(NO_3)_2{\cdot}6H_2O$ were stirred (*ca.* 500 rpm) at 343 K while dropwise adding 200 cm^3 of a 0.32 M aqueous solution of $(NH_4)_2CO_3$ (Sigma-Aldrich, 98%). The resulting slurry was aged for 2 h at the same temperature under magnetic stirring. Finally, the precipitate was isolated by high-pressure filtration, washed 3 times with deionized water (1 L each time), dried in a vacuum oven (2 kPa, 338 K, 12 h), and calcined at 773 K (2 K min^{-1}) for 3 h in static air.

Reduced catalysts were obtained by treating samples (*ca.* 0.1 g) in a 70 cm^3_{STP} min^{-1} flow of 10 vol.% H_2 in Ar (Messer, purity 5.0) for 2 h at 573 K (2 K min^{-1}) under ambient pressure.

Catalyst characterization

Inductively coupled plasma optical emission spectroscopy (ICP-OS) was conducted using a Horiba Ultra 2 instrument equipped with a photomultiplier tube detector. Samples were dissolved in hot *aqua regia* (353 K) during 12 h prior to the analysis, except for zirconia-containing materials. The latter were digested using a mixture of HNO_3 (Sigma-Aldrich, 65 wt.%), H_2SO_4 (Alfa Aesar, 95 wt.%), and HF (Sigma-Aldrich, 48 wt.%) with a volume ratio of 2:1:1 for 72 h, followed by neutralization with a saturated solution of boric acid (Fluka, 99%). Nitrogen sorption at 77 K was carried out using a Micromeritics TriStar II analyzer. Prior to the measurements, samples were degassed under vacuum (*ca.* 10 Pa) at 473 K for 12 h. The total surface area (S_{BET}) was determined using the Brunauer–Emmett–Teller (BET) method. The copper surface area and dispersion were determined by pulsed titration with N_2O at ambient pressure using a Micromeritics AutoChem HP II analyzer coupled to a Pfeiffer OMNI^{Star} mass spectrometer (MS). Samples were loaded into a stainless steel tube, exposed to 10 vol% H_2 in Ar at 573 K (5 K min^{-1}) for 2 h to ensure complete copper reduction, and then purged with He. The copper surface was subsequently oxidized at 363 K using pulses of 10 vol.% N_2O in He. The copper surface area was calculated using a mean surface density of copper atoms of 1.47×10^{19} m^{-2}. X-ray diffraction (XRD) was measured in a PANalytical X'Pert PRO-MPD diffractometer operated in the Bragg–Brentano geometry using Ni-filtered Cu Kα radiation (λ = 0.1541 nm). Data was acquired in the 10−70° 2θ range with an angular step size of 0.025° and a counting time of 12 s per step. High-angle annular dark field scanning transmission electron microscopy (HAADF-STEM) coupled to energy-dispersive X-ray spectroscopy (EDX)was performed using a Talos F200X instrument operated at 200 kV and equipped with a FEI SuperX detector. Temperature-programmed reduction with CO (CO-TPR) was conducted at ambient pressure using a Micromeritics AutoChem HP II coupled to a Pfeiffer OMNI^{Star} MS. Samples were loaded into a stainless steel tube, dried at 423 K in He for 1 h (10 K min^{-1}), and cooled down to 273 K (20 K min^{-1}) using dry ice in ethanol. The temperature-programmed reduction was then carried out using 1 vol% CO in He (Messer, CO 4.7 in He 5.0) and increasing the temperature to 873 K (5 K min^{-1}). X-ray photoelectron spectroscopy (XPS) was performed in a Physical Electronics (PHI) Quantum 2000 X-ray photoelectron spectrometer using monochromatic Al Kα radiation generated from an electron beam operated at 15 kV and 32.3 W and a hemispherical capacitor electron-energy analyzer, equipped with a channel plate and a position-sensitive detector. Samples were firmly pressed onto indium foil patches, which were then mounted onto a sample platen and introduced into the spectrometer. Analyses were conducted under ultra-high vacuum conditions (residual pressure = 5×10^{-8} Pa) with an electron take-off angle of 45°, operating the analyzer in the constant pass energy mode.

Catalytic evaluation

The gas-phase hydrogenation of CO_x (CO_x = CO+CO_2) to methanol was performed in a PID Eng&Tech high-pressure continuous-flow setup comprising four parallel fixed-bed reactors (internal diameter = 4 mm) described previously.[8] Undiluted catalysts (mass (w_{cat}) = 0.1 g, particle size = 0.2–0.3 mm) were loaded into each reactor, held in place by a quartz-wool bed set on a quartz frit, and purged with a 80 cm^3_{STP} min^{-1} flow of He (Pangas, purity 4.6) for 30 min at ambient pressure. Under the same flow, the pressure was increased to 5.5 MPa for a leak test. Prior to the reaction, catalysts were reduced in a 70 cm^3_{STP} min^{-1} flow of 10 vol.% H_2 in Ar (Messer, 5.0) for 2 h at ambient pressure at 573 K (2 K min^{-1}). Thereafter, the reactors were cooled down to the desired reaction temperature and the reaction was carried out by feeding a mixture of H_2, CO (Messer, 5.0), and CO_2 (20 vol.% in H_2, Messer, 4.5), with a molar H_2/CO_x ratio of 4 at 513 K (593 K for ZnO-ZrO_2), 5 MPa, and a weight hourly space velocity (*WHSV*) of 48,000 cm^3_{STP} h^{-1} g_{cat}^{-1}, unless stated otherwise. The impact of CO on the catalyst performance was assessed by means of CO_2-CO cycle experiments, which are graphically depicted in Figure 2. During full cycles (FC, Figure 2a), CO_2 in the feed was progressively replaced by CO from *R* (*R* = CO/CO_x, with CO_x = CO + CO_2) equal 0 to 0.5 in steps of 0.1 and then replenished by replacing CO in an analogous manner, while maintaining a constant molar H_2/CO_x ratio of 4. Reverse full cycles were performed similarly to FC but starting at and returning to *R* = 0.5 (rFC, Figure 2b). Half-cycles (HC, Figure 2c) were conducted starting at *R* = 0 and increasing the CO concentration to reach *R* = 0.5. The same step size of 0.1 was kept as in full cycles.

Response factors (F_i) for each compound *i* in the effluent stream, respective to the internal standard (20 vol.% C_2H_6 in He, Messer, purity 3.5), in gas chromatographic analysis were determined by Eq. 1, where A_i is the integrated area determined for the peak of compound *i* and n_i^{in} is the corresponding known molar flow at the reactor inlet.

$$F_i = \frac{A_{C_2H_6} / n^{in}_{C_2H_6}}{A_i / n_i^{in}} \quad (1)$$

Their values were calculated using the average of 5 points around the expected concentration of the respective analyte. The unknown effluent molar flow and methanol production rate (r_{MeOH}) were determined using Eqs. 2 and 3, respectively.

$$n_i^{out} = \frac{A_i \times F_i}{A_{C_2H_6}} \times n^{out}_{C_2H_6} \quad (2)$$

$$r_{MeOH} = \frac{n^{out}_{MeOH}}{w_{cat}},\ \mathrm{mol}_{MeOH}\ h^{-1}\ g_{cat}^{-1} \quad (3)$$

The methanol space-time yield (*STY*) was determined as the product of r_{MeOH} and the molar weight of methanol. Data reported corresponds to the average of 4 measurements preceding a specific time on stream. The carbon balance (ε_c)was determined for each experiment according to Eq. 4 and was always higher than 95%.

$$\varepsilon_c = \left(1 - \frac{n^{out}_{CO_2} + n^{out}_{MeOH} + n^{out}_{CO}}{n^{in}_{CO_2} + n^{in}_{CO}}\right) \times 100, \% \quad (4)$$

All data related to indium oxide-based systems were taken from our recent publication.[8]

Acknowledgements

The Scientific Center for Optical and Electron Microscopy (ScopeM) at the ETH Zurich is acknowledged for the use of their facilities.

Keywords: methanol synthesis • heterogeneous catalysts • hydrogenation • carbon dioxide • hybrid feeds

[1] a) X. Jiang, X. Nie, X. Guo, C. Song, J. G. Chen, *Chem. Rev.* **2020**, *120*, 7984–8034; b) I. Yarulina, A. D. Chowdhury, F. Meirer, B. M. Weckhuysen, J. Gascon, *Nat. Catal.* **2018**, *1*, 398–411; c) G. A. Olah, *Angew. Chem. Int. Ed.* **2013**, *52*, 104–107; *Angew. Chem.* **2013**, *125*, 112–116.

[2] a) A. González-Garay, M. S. Frei, A. Al-Qahtani, C. Mondelli, G. Guillén-Gosálbez, J. Pérez-Ramírez, *Energy Environ. Sci.* **2019**, *12*, 3425–3436; b) A. Goeppert, M. Czaun, J.-P. Jones, G. K. Surya Prakash, G. A. Olah, *Chem. Soc. Rev.* **2014**, *43*, 7995–8048.

[3] a) M. Jouny, G. S. Hutchings, F. Jiao, *Nat. Catal.* **2019**, *2*, 1062–1070; b) J. Zhong, X. Yang, Z. Wu, B. Liang, Y. Huang, T. Zhang, *Chem. Soc. Rev.* **2020**, *49*, 1385–1413; c) J. Artz, T. E. Müller, K. Thenert, J. Kleinekorte, R. Meys, A. Sternberg, A. Bardow, W. Leitner, *Chem. Rev.* **2018**, *118*, 434–504.

[4] a) D. Laudenschleger, H. Ruland, M. Muhler, *Nat. Commun.* **2020**, *11*, 3898-3902; b) J. Nakamura, T. Uchijima, Y. Kanai, T. Fujitani, *Catal. Today* **1996**, *28*, 223–230; c) J. Nakamura, T. Fujitani, S. Kuld, S. Helveg, I. Chorkendorff, J. Sehested, *Science* **2017**, *357*, 1296–1299; d) J. Ye, C. Liu, D. Mei, Q. Ge, ACS Cata*l.* **2013**, *3*, 1296–1306; e) M. Behrens, F. Studt, I. Kasatkin, S. Kühl, M. Hävecker, F. Abild-pedersen, S. Zander, F. Girgsdies, P. Kurr, B. Kniep, *Science* **2012**, *759*, 893–898; f) O. Martin, C. Mondelli, A. Cervellino, D. Ferri, D. Curulla-Ferré, J. Pérez-Ramírez, *Angew. Chem. Int. Ed.* **2016**, *55*, 11031–11036; *Angew. Chem.* **2016**, *128*, 11197–11202.

[5] a) Y. Wang, S. Kattel, W. Gao, K. Li, P. Liu, J. G. Chen, H. Wang, *Nat. Commun.* **2019**, *10*, 1166; b) K. Li, J. G. Chen, *ACS Catal.* **2019**, *9,* 7840–7861.

[6] a) O. Martin, A. J. Martín, C. Mondelli, S. Mitchell, T. F. Segawa, R. Hauert, C. Drouilly, D. Curulla-Ferré, J. Pérez-Ramírez, *Angew. Chem. Int. Ed.* **2016**, *55*, 6261–6265; *Angew. Chem.* **2016**, *128*, 6369–6373; b) M. S. Frei, M. Capdevila-Cortada, R. García-Muelas, C. Mondelli, N. López, J. A. Stewart, D. Curulla Ferré, J. Pérez-Ramírez, *J. Catal.* **2018**, *361*, 313–321; c) M. M. Li, H. Zou, J. Zheng, T. Wu, T. Chan, Y. Soo, X. Wu, X. Gong, T. Chen, K. Roy, G. Held, S. M. E. Tsang, *Angew. Chem. Int. Ed.* **2020**, *59*, 16039-16046 ; *Angew. Chem.* **2020**, *132*, 16173-16180; d) A. Pustovarenko, A. Dikhtiarenko, A. Bavykina, L. Gevers, A. Ramírez, A. Russkikh, S. Telalovic, A. Aguilar, J.-L. Hazemann, S. Ould-Chikh, et al., *ACS Catal.* **2020**, *10*, 5064–5076; e) S. Dang, B. Qin, Y. Yang, H. Wang, J. Cai, Y. Han, S. Li, P. Gao, Y. Sun, *Sci. Adv.* **2020**, *6*, 2060; f) T. Y. Chen, C. Cao, T. B. Chen, X. Ding, H. Huang, L. Shen, X. Cao, M. Zhu, J. Xu, J. Gao, et al., *ACS Catal.* **2019**, *9*, 8785–8797; g) M. S. Frei, C. Mondelli, A. Cesarini, F. Krumeich, R. Hauert, J. A. Stewart, D. Curulla Ferré, J. Pérez-Ramírez, *ACS Catal.* **2020**, *10*, 1133–1145; h) T. Numpilai, P. Kidkhunthod, C. K. Cheng, C. Wattanakit, M. Chareonpanich, J. Limtrakul, T. Witoon, *Catal. Today* **2020**, DOI 10.1016/j.cattod.2020.03.011; i) J. L. Snider, V. Streibel, M. A. Hubert, T. S. Choksi, E. Valle, D. C. Upham, J. Schumann, M. S. Duyar, A. Gallo, F. Abild-Pedersen, et al., *ACS Catal.* **2019**, *9*, 3399–3412; j) M. S. Frei, C. Mondelli, R. García-Muelas, K. S. Kley, B. Puértolas, N. López, O. V. Safonova, J. A. Stewart, D. Curulla Ferré, J. Pérez-Ramírez, *Nat. Commun.* **2019**, *10*, 3377; l) N. Rui, Z. Wang, K. Sun, J. Ye, Q. Ge, C. jun Liu, *Appl. Catal. B* **2017**, *218*, 488–497; m) N. Rui, F. Zhang, K. Sun, Z. Liu, W. Xu, E. Stavitski, S. D. Senanayake, J. A. Rodriguez, C.-J. Liu, *ACS Catal.* **2020**, *10*, 11307−11317.

[7] a) J. Wang, G. Li, Z. Li, C. Tang, Z. Feng, H. An, H. Liu, T. Liu, C. Li, *Sci. Adv.* **2017***, 3*, 1701290; b) C. Temvuttirojn, Y. Poo-Arporn, N. Chanlek, C. K. Cheng, C. C. Chong, J. Limtrakul, T. Witoon, *Ind. Eng. Chem. Res.* **2020**, *59*, 5525–5535.

[8] T. P. Araújo, A. Shah, C. Mondelli, J. A. Stewart, D. Curulla Ferré, J. Pérez-Ramírez, *Appl. Catal. B* **2021**, *285*, 119879.

[9] a) O. Martin, J. Pérez-Ramírez, *Catal. Sci. Technol.* **2013**, *3*, 3343–3352; b) O. Martin, C. Mondelli, D. Curulla-Ferré, C. Drouilly, R. Hauert, J. Pérez-Ramírez, *ACS Catal.* **2015**, *5*, 5607–5616.

[10] a) A. Goeppert, M. Czaun, G. K. Surya Prakash, G. A. Olah, *Energy Environ. Sci.* **2012**, *5*, 7833; b) D. Cebrucean, V. Cebrucean, I. Ionel, *Energy Procedia* **2014**, *63*, 18–26; c) R. T. J. Porter, M. Fairweather, M. Pourkashanian, R. M. Woolley, *Int. J. Greenh. Gas Control* **2015**, *36*, 161–174; d) M. Asadullah, *Renew. Sustain. Energy Rev.* **2014**, *40*, 118–132; e) N. Couto, A. Rouboa, V. Silva, E. Monteiro, K. Bouziane, *Energy Procedia* **2013**, *36*, 596–606.

[11] a) Y. Yang, C. A. Mims, D. H. Mei, C. H. F. Peden, C. T. Campbell, *J. Catal.* **2013**, *298*, 10–17; b) R. Gaikwad, H. Reymond, N. Phongprueksathat, P. Rudolf Von Rohr, A. Urakawa, *Catal. Sci. Technol.* **2020**, *10*, 2763–2768; c) Y. Zhang, Q. Sun, J. Deng, D. Wu, S. Chen, *Appl. Catal. A* **1997**, *158*, 105–120.

[12] U. Ash-Kurlander, O. Martin, L. D. Fontana, V. R. Patil, M. Bernegger, C. Mondelli, J. Pérez-Ramírez, A. Steinfeld, *Energy Technol.* **2016**, *4*, 565–572.

[13] A. Tsoukalou, P. M. Abdala, A. Armutlulu, E. Willinger, A. Fedorov, C. R. Müller, *ACS Catal.* **2020**, *10*, 10060–10067.

[14] V. Dybbert, S. M. Fehr, F. Klein, A. Schaadt, A. Hoffmann, E. Frei, E. Erdem, T. Ludwig, H. Hillebrecht, I. Krossing, *Angew. Chem. Int. Ed.* **2019**, *58*, 12935–12939; *Angew. Chem.* **2019**, *131*, 13069–13073.

[15] A. Tsoukalou, P. M. Abdala, D. Stoian, X. Huang, M. G. Willinger, A. Fedorov, C. R. Müller, *J. Am. Chem. Soc.* **2019**, *141*, 13497–13505.

Entry for the Table of Contents

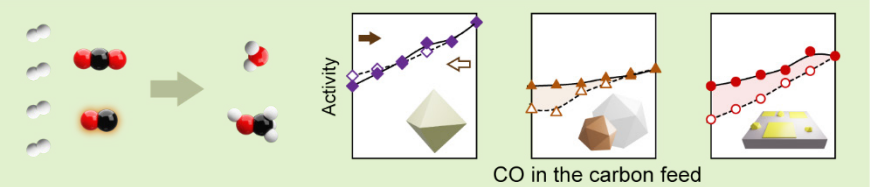

CO gives and takes: The impact of CO on copper and ZnO-ZrO_2 catalysts for CO_2-to-methanol is assessed in cycle tests with hybrid CO_2-CO feeds and contrasted to In_2O_3-based systems. CO addition promotes all catalyst families for structural and mechanistic reasons. Mild-to-moderate deactivation is observed upon its removal for copper- and In_2O_3-based catalysts due to sintering, while ZnO-ZrO_2 stands out for its fully reversible behavior.

Institute and/or researcher Twitter usernames: @catalysis_eth